



Research on degradation of polysaccharides during *Hericium erinaceus* fermentation

Yue Su, Hongxuan Li, Ziyu Hu, Yu Zhang, Ling Guo, Meili Shao, Chaoxin Man^{**}, Yujun Jiang^{*}

Key Laboratory of Dairy Science, Ministry of Education, Department of Food Science, Northeast Agricultural University, Harbin, 150030, China

ARTICLE INFO

Keywords:

Lactobacillus gasseri JM1
Fermentation
Degradation
Polysaccharide
Structure characterization

ABSTRACT

The most common type of fermentation that can change the physicochemical properties and biological activity of polysaccharide is caused by lactic acid bacteria. In this paper, the structures of *Lactobacillus gasseri* JM1 degraded and undegraded *Hericium erinaceus* polysaccharides (FHEP and HEP) were characterized, and the biological activities of the polysaccharides were determined. The result showed that polysaccharide molecular weight and monosaccharide composition changes due to fermentation degradation. FHEP had a molecular weight of 3.5×10^4 Da, which was lesser than the molecular weight of HEP (7.5×10^7 Da). HEP was composed of nine types of monosaccharides, while FHEP contained six types of monosaccharides. The results of methylation and NMR analysis results showed that after the structural link of HEP was degraded, it became FHEP, which has a branched structure. In vitro antioxidant activities and three enzyme-inhibitory activities found that FHEP had significantly higher activity than HEP ($P < 0.05$), indicating that the degraded polysaccharides have better biological activity.

1. Introduction

Lactic acid bacteria are primarily Gram-positive bacteria with different morphology, metabolic properties and physiological characteristics (Ma et al., 2021; Yang, Ren, & Li, 2022). Using lactic acid bacteria as an expression system is safe, non-endotoxin, and exogenous (Amarita, Requena, Taborda, Amigo, & Pelaez, 2001). Lactic acid bacteria can be used in fermentation to produce healthy foods for humans and animals (Zhang et al., 2021). Lactic acid bacteria fermentation naturally alters the nutritional properties of foods and food ingredients (Marco et al., 2017). This process increases the availability of biologically active substrates while enhancing the uptake and absorption rate of the substrates in the human body. Therefore, the fermentation process has several health benefits. For example, fermentation by lactic acid bacteria can cause the degradation of polysaccharides structure and biological activity (Gao et al., 2018).

Mushrooms and their extracts have various compounds that promote nutrition and health (Mingyi, Belwal, Devkota, Li, & Luo, 2019). Over 2000 distinct types of mushrooms have been identified (Yang, Cui, Li, Man, & Jiang, 2021). Among them, *Hericium erinaceus* is a kind of "Medicine and food homology" that is widely distributed in nature (Yu et al., 2021). It is rich in nutrients and has been used for hundreds of

years in traditional Chinese medicine to treat gastritis. Phytochemical studies have revealed that its main components are hericin, hericine and hericium polysaccharides, with various biological activities, including immunomodulatory, antibacterial, anti-tumor, and antioxidant. (Ryu et al., 2021). The polysaccharide of *Hericium erinaceus* polysaccharide was thought to be its main active ingredient. It has drawn the attention of researchers as a functional food because of its numerous health-promoting functions. Polysaccharides are natural or synthetic macromolecular compounds formed by the polymerization of one or more types of monosaccharides through covalent glycosidic bond. Polysaccharides have been extensively researched and used in foods as non-toxic, widely sourced, and micro-high-efficiency natural extracts. Numerous studies have shown that polysaccharides have antioxidant, hypoglycemic, and other properties. (Pei, Cao, Wang, Ren, & Ge, 2022; Zhu et al., 2022). After protein engineering and genetic engineering, glycoengineering centered on the function, structure, and medicinal use of polysaccharides is regarded as the final scientific frontier in biochemistry and molecular biology. These macromolecules have been used as non-toxic ingredients for developing functional products in agriculture, health food, cosmetics, and the medical industry (Chen, Ji, Xu, & Liu, 2019).

Few studies had been conducted on the degradation of fungal

* Corresponding author.

** Corresponding author.

E-mail addresses: mcxwh2006@qq.com (C. Man), yujun_jiang@163.com (Y. Jiang).

polysaccharides by lactic acid bacteria. In this study, we combined high-performance liquid chromatography (HPLC), Fourier Infrared spectroscopy (FT-IR), Nuclear Magnetic Resonance (NMR), and scanning electron microscopy (SEM) to analyze and detect polysaccharides molecular weight, monosaccharide composition, glycosidic bond type, linkage mode, and apparent structure. The characterization of the structure and biological activity of *Hericium erinaceus* polysaccharides after fermentation by *Lactobacillus gasseri* JM1 were compared. This study provided a basis for the further development and utilization of *Hericium erinaceus* resources.

2. Materials and method

2.1. Materials and reagents

Hericium erinaceus was purchased from a local market in Dongning City (Heilongjiang, China); MRS Broth was purchased from Qingdao Haibo Biotechnology Co., Ltd. (Qingdao, China); PNPG, α -glucosidase, α -amylase, purchased from Soleibao (Beijing, China); Acarbose purchased from Shanghai Yuanye Co., Ltd. (Shanghai, China); Monosaccharide standards (Fucose, Rhamnose, Arabinose, Galactose, Glucose, Xylose, Mannose, Fructose, Ribose, Galacturonic Acid, Glucuronic Acid, Mannuronic Acid, Guluronic Acid) were purchased from sigma-Aldrich (USA).

2.2. Bacterial strain and growth condition

Lactobacillus gasseri JM1 (Preserved by Key Laboratory of Dairy Science, Ministry of Education, Northeast Agricultural University). 16S rDNA sequence was determined for bacterial identification and uploaded to National Center for Biotechnology Information (NCBI). The strains were activated and preserved, and articles related to the results of Whole-Genome sequencing were published by Sun et al. (Sun et al., 2020).

2.3. Extraction of polysaccharides

Refer to Gao and Zhang et al. (Gao et al., 2018; Zhang et al., 2018), who slightly modified the *Asparagus officinalis* polysaccharide and used *Lactobacillus plantarum* fermentation, the *Hericium erinaceus* was crushed through a 100-mesh sieve for use. Without any nutritional supplements, *Lactobacillus gasseri* JM1 was inoculated into the solution at 1×10^8 CFU/mL, using *Hericium erinaceus* powder and distilled water as the medium. The material-to-liquid ratio was 1:20. Shaking was used to cultivate the fermented *Hericium erinaceus* solution for 48 h at 37 °C. After fermentation, the solution was sterilized and freeze-dried into powder.

5.00 g of lyophilized powder was added to 100 mL of distilled water in a beaker, and the mixture was magnetically stirred (350 r/min) for 3.5 h (85 °C), before centrifuging (4500 g, 10 min). Used three times the volume of precipitate the supernatant with anhydrous ethanol (95%) and keep it for 12 h. The obtained precipitate was centrifuged at 4500 g for 10 min to obtain the crude polysaccharide. The protein was removed by the TCA method (the final concentration of TCA in the solution is 20% (W/V)), and the color was and removed using a 3% hydrogen peroxide solution. To obtain *Hericium erinaceus* polysaccharide degraded by fermentation, we used a dialysis bag with molecular weight cut-off 8000–14000Da, dialyzed with distilled water for 48 h, and lyophilized. The extraction steps of undegraded polysaccharides were the same as those of the degraded polysaccharides during the fermentation process of *Hericium erinaceus* except that no bacterial liquid is added.

2.4. Determination of polysaccharide content

The phenol-sulfuric acid method was used to determine the content of polysaccharides in agaric polysaccharides.

2.5. Structural characterization of polysaccharides

2.5.1. UV-vis spectroscopic analysis

The polysaccharide was prepared as a 1 mg/mL solution, and 200–800 nm ultraviolet scanning was conducted using an ultraviolet-visible spectrophotometer.

2.5.2. Determination of molecular weight

The gel chromatography-differential-multi-angle laser light scattering system was used, based on for the nature of the compound, using a gel exclusion chromatography column with a suitable molecular weight range (Ohpak SB-805 HQ).

2.5.3. Determination of monosaccharide composition

Thermo ICS5000 (Thermo Fisher Scientific, USA) ion chromatography system was used, and an electrochemical detector was used to analyze and detect the electrochemical detector.

2.5.4. FT-IR analysis

A dried polysaccharide sample weighing 2 mg was combined with 150 mg of pure KBr, mixed with it, and pressed into slices. Using an FT-IR spectrometer (Nicolet iS50, Germany), infrared spectrum scanning was done in the range of 4000–500 cm^{-1}

2.5.5. Observation of the microstructure

Scanning electron microscopy was used to detect polysaccharides (HITACHI S-3400N, Japan). The samples were fixed to the sample holder, gold was applied, and then, the samples were observed at 15000 \times .

The morphology of the polysaccharides was examined using an atomic force microscope (AFM, Bruker AXS, Germany).

2.6. Structural identification of polysaccharides

2.6.1. Methylation analysis

The polysaccharides were derivatized using the method described by Chen et al. (Chen, Wang, Zhang, Zhang, & Linhardt, 2021). The final derivative was injected into the GC-MS system for detection.

2.6.2. NMR determination

The method described by Huang et al. (Huang et al., 2019). was slightly modified. The polysaccharide was dissolved in 500 μL of D_2O , to a final concentration that was greater than or equal to 30 mg/mL, and added to the NMR (AVANCEIII HD, Germany) tube, followed by 1D NMR and 2D NMR spectrometer scanning.

2.7. Molecular modeling methods

Based on a study by Zhang et al. (Zhang, Wang, Guo, Wang, & Cui, 2020), the polysaccharide structure was computer-simulate. The structures of the two polysaccharides were obtained by computer-simulate analysis, and geometry optimization was performed using Insight II/Discover_3 and RIS programs (version 4.0.0, Molecular Simulations Inc., San Diego, USA) using a silicon graphics O2 workstation. Using the Discover_3 module and the RIS module in the RMCC method to deduce the conformational parameters of the polysaccharide, the conformation of the polysaccharide was finally simulated.

2.8. Biological activity of polysaccharides

2.8.1. Antioxidant activity determination

The antioxidant activity of polysaccharides method described in another study (Su & Li, 2020).

2.8.2. Determination of enzyme inhibition activity

Reference to the research method of Li et al. (Li, Su, Feng, & Hong,

2020). Acarbose was used as a control to determine the inhibitory effect of polysaccharides on α -glucosidase and α -amylase. According to the Yuan et al. research method, a polysaccharide solution with a concentration of 10 mg/mL was used to study the inhibitory effect of polysaccharide (Yuan et al., 2018).

2.9. Statistical analysis

Data are presented as the mean \pm standard deviation (Mean \pm SD). The statistical software IBM SPSS 23 was used for conducting ANOVA, and Origin 2018 was used to draw plots. Chromatographic data were processed using ASTRA 6.1 and the Chrome Leon software. All experiments were replicated in thrice.

3. Results and discussion

3.1. Analysis of the physicochemical properties of polysaccharides

HEP and FHEP both had yields of 2.4% and 3.7%, respectively. The polysaccharide contents of HEP and FHEP were 98.08% and 93.51%, respectively, and the purity was greater than 90%, which ensured subsequent analysis of the polysaccharide structure.

3.2. Structural features analysis of polysaccharides

3.2.1. UV scan analysis

UV spectrum scan of HEP and FHEP (Fig. 1a) showed no peak at 260 nm and 280 nm, indicating that the two polysaccharides lacked nucleic acids and proteins.

3.2.2. Molecular weight and monosaccharide composition

The molecular weight of HEP and FHEP were measured using a gel chromatography-differential-multi-angle laser light scattering system and a gel exclusion chromatography column (Fig. 2). The molecular weight of HEP and FHEP were 7.5×10^7 Da and 3.5×10^4 Da, respectively. The dispersibility index was 2.163 and 1.328 respectively, indicating that the polymer chains were of different lengths.

HEP was mainly composed of 9 kinds of monosaccharides: fucose, arabinose, galactose, glucose, xylose, mannose, ribose, glucuronic acid and mannuronic acid, and their ratio was 7.90: 0.28: 24.18: 56.74: 2.30: 5.87: 1.00: 1.27: 0.46. FHEP was mainly composed of six kinds of monosaccharides: fucose, arabinose, galactose, glucose, mannose and glucuronic acid, and their ratio was 3.96: 0.14: 12.54: 80.68: 1.33: 1.35 (Table 1).

Due to the fermentation by *Lactobacillus gasseri* JM1, the molecular weight and monosaccharides decreased. Studies had found that lactic acid bacteria utilize carbohydrate substrates through carbohydrate active enzymes (CAZy). Therefore, it was speculated that these CAZy catalyze the hydrolysis of polysaccharides and lower the molecular

weight during fermentation (Gao et al., 2018). In parallel, the laboratory conducted a whole genome sequencing of *Lactobacillus gasseri* JM1 strain in the early stage and found that it could be classified into 22 functional categories using the Clusters of Orthologous Groups (COG) database, with carbohydrate metabolism making up 10.4% of the categories (Sun et al., 2020). Thirty-eight coding genes were involved in the phosphotransferase system (PTS) and 142 coding genes involved in the transport and metabolism of carbohydrates. PTS takes part in various sugar transport in this strain, including fructose, mannose, galactose and so on. This may also be why FHEP contains less mannose and galactose than HEP.

3.2.3. FT-IR of analysis

An efficient technique for examining the structure of polysaccharides is Infrared spectroscopy. It is possible to deduce the possible structural characteristics from the absorption peaks of polysaccharides (Chi et al., 2018). As showed in Fig. 1b, the spectrum appearing at the peak of $3300\text{--}3400\text{ cm}^{-1}$ was caused by polysaccharide O–H stretching vibration (Ji, Yan, Hou, Shi, & Liu, 2019). The peak appearing near 2900 cm^{-1} was caused by C–H stretching (Niu et al., 2020). The peak at $1600\text{--}1710\text{ cm}^{-1}$ was due to C=O tensile vibration (Niu et al., 2020). The peak at $1475\text{--}1300\text{ cm}^{-1}$ was the vibration peak of the C–H bond, indicating the deformation of the CH_2 group. The peak around $1150\text{--}1010\text{ cm}^{-1}$ was attributed to the stretching vibration of the pyranose ring of glucosyl residues, and $900\text{--}500\text{ cm}^{-1}$ contains the α configuration (Zhu et al., 2021). It showed that both sugars contain α -configuration pyranose. There were differences between the two polysaccharides between 500 and 1600 cm^{-1} , HEP at 1080 and 1040 cm^{-1} contains the C–OH (Li et al., 2021). This was consistent with the results of the monosaccharide composition. FHEP had a unique peak that appears might had the presence of methyl or S=O group at 1204 cm^{-1} (Wang et al., 2022). This might bring better biological activity to polysaccharides, and research had shown that the biological activity of polysaccharides was related to its structural changes (Gao et al., 2018).

3.2.4. Analysis of microstructure

SEM is an important tool for characterizing the structure of polysaccharides. AFM is a technique that does not require complicated sample pretreatment and can be used to observe the surface morphology of biological macromolecules, and thus, has become a popular tool in the characterization of polysaccharides (Wu & Huang, 2021). Fig. 3 displayed the findings from SEM and AFM results of the two polysaccharides.

A large flaky structure with a smooth surface was observed in the morphology of HEP observed by SEM at the same magnification. Contrarily, FHEP exhibited a small, fragmented structure, due to changes in the morphology and structure of polysaccharides caused by fermentation.

Using AFM, two polysaccharides' surface morphology was observed.

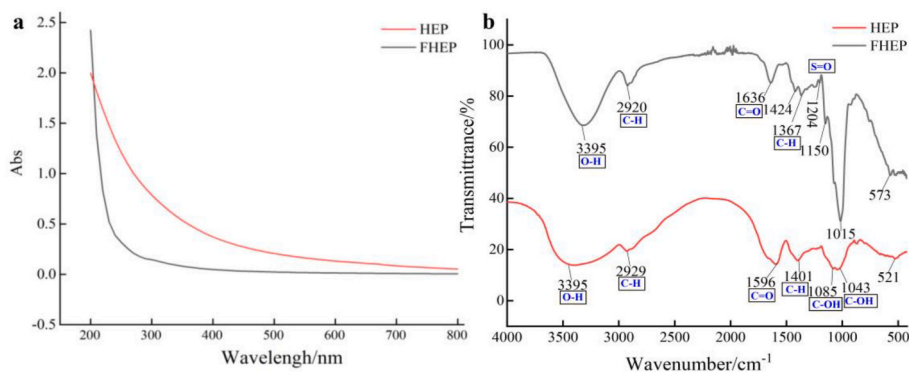


Fig. 1. The UV and FT-IR spectrum of polysaccharides (a) UV, (b) FT-IR.

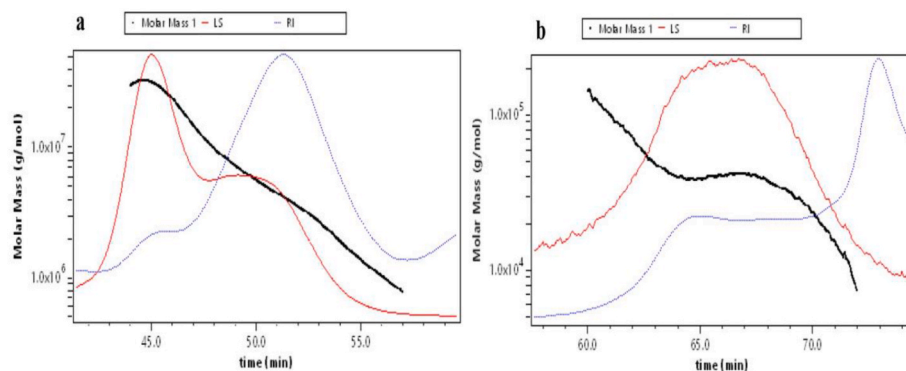


Fig. 2. The gel permeation chromatogram of HEP and FHEP. (a) HEP, (b) FHEP.

Table 1
Molecular weight and monosaccharide composition of polysaccharides.

	HEP	FHEP
Molecular weight		
Mw/Da	7.5×10^7	3.5×10^4
Mw/Mn	2.163	1.328
Monosaccharide composition		
Fucose/%	7.90	3.96
Arabinose/%	0.28	0.14
Galactose/%	24.18	12.54
Glucose/%	56.74	80.68
Xylose/%	2.30	–
Mannose/%	5.87	1.33
Ribose/%	1.00	–
Glucuronic Acid/%	1.27	1.35
Mannuronic Acid/%	0.46	–

Note: (–) stands not detected.

From the topography perspective, HEP appeared as an amorphous, multi-branched network structure in the solution. Various side chains in the structure cross-linking between glycogens to form bonds of different sizes. The FHEP seemed to have a spherical structure with irregular edges. The average single chain diameter of polysaccharides was between 0.1 and 1 nm (Wang, Zhang, Xiao, & MACROMOL, 2010). A single

strand of HEP had a larger diameter ($\sim 92.6\text{--}3\text{ nm}$) than a single strand of FHEP ($3\text{--}3.6\text{ nm}$). The R_{\max} , R_q , and R_a values of HEP were 17 nm, 0.831 nm and 0.502 nm, respectively, while the R_{\max} , R_q , and R_a values of FHEP were 11.5 nm, 0.514 nm and 0.166 nm, respectively. These results showed that the surface of HEP was rougher than FHEP.

3.3. Analysis of polysaccharide bonding structure

3.3.1. Methylation analysis

Methylation analysis is commonly used method to determine the linkage structure of complex carbohydrates. The method includes derivatizing the single component sugars of polysaccharides into partially methylated alditol acetates (PMAA), and analyzing and quantifying them by gas chromatography-mass spectrometry (Sims, Carnachan, Bell, & Hinkley, 2018).

The PMAAs were identified by their retention times of the TIC GC peaks (Figs. 4–5) and their EI-mass spectra, which were compared to the CCRC database (<https://www.ccrcc.uga.edu/specdb/ms/pmaa/pframe.html>). The inferred linking modes were inferred were showed in Table 2. This was similar to the result of monosaccharide composition. The analysis of monosaccharide composition indicated that, some undetected residues might result from the loss caused by the hydrolysis, reduction and acetylation during the sample determination process (Qu, Gao, Zhao, Wang, & Yi, 2019).

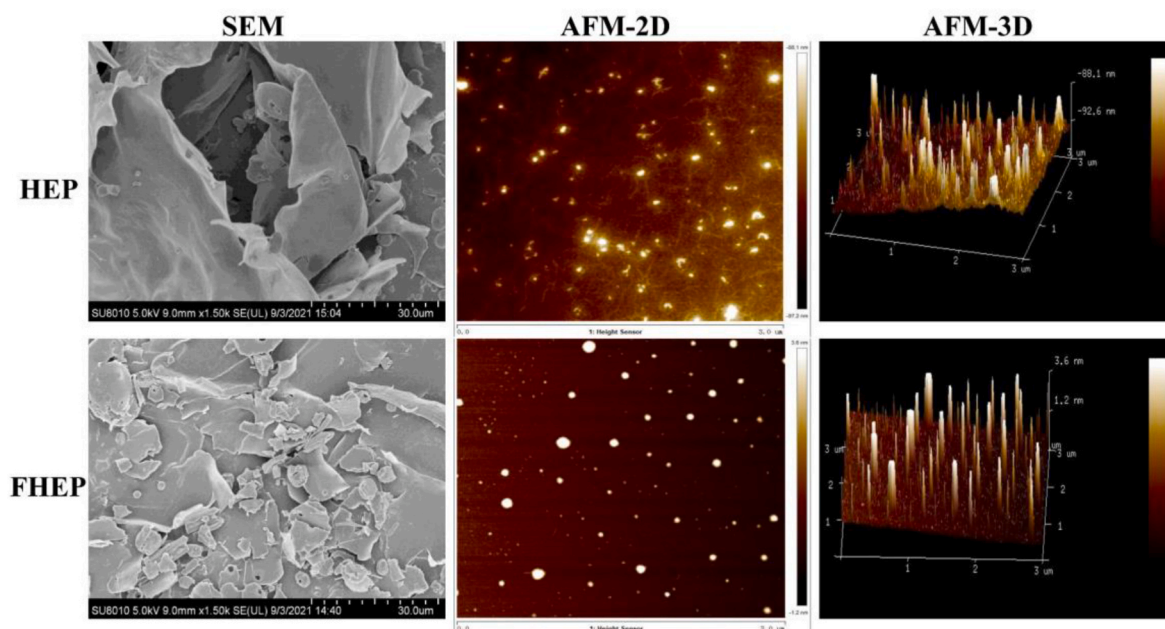


Fig. 3. SEM and AFM of polysaccharide.

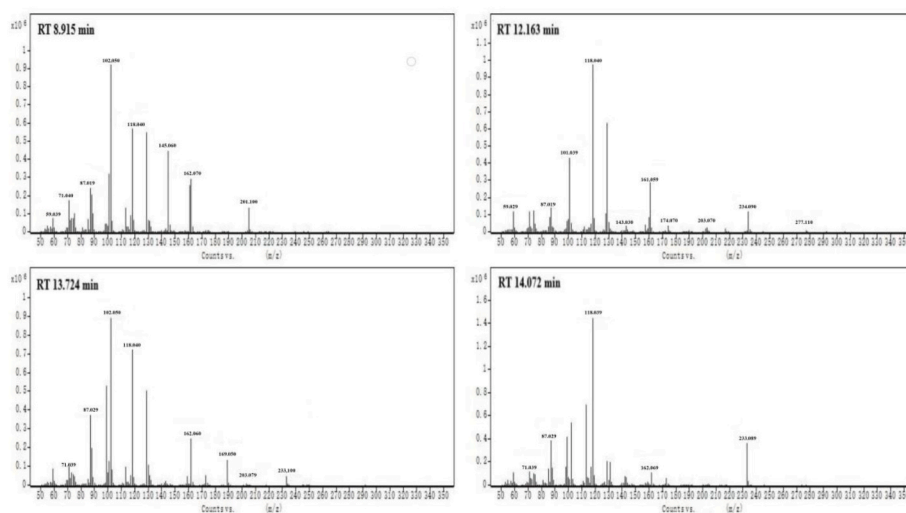


Fig. 4. Methylation results of HEP.

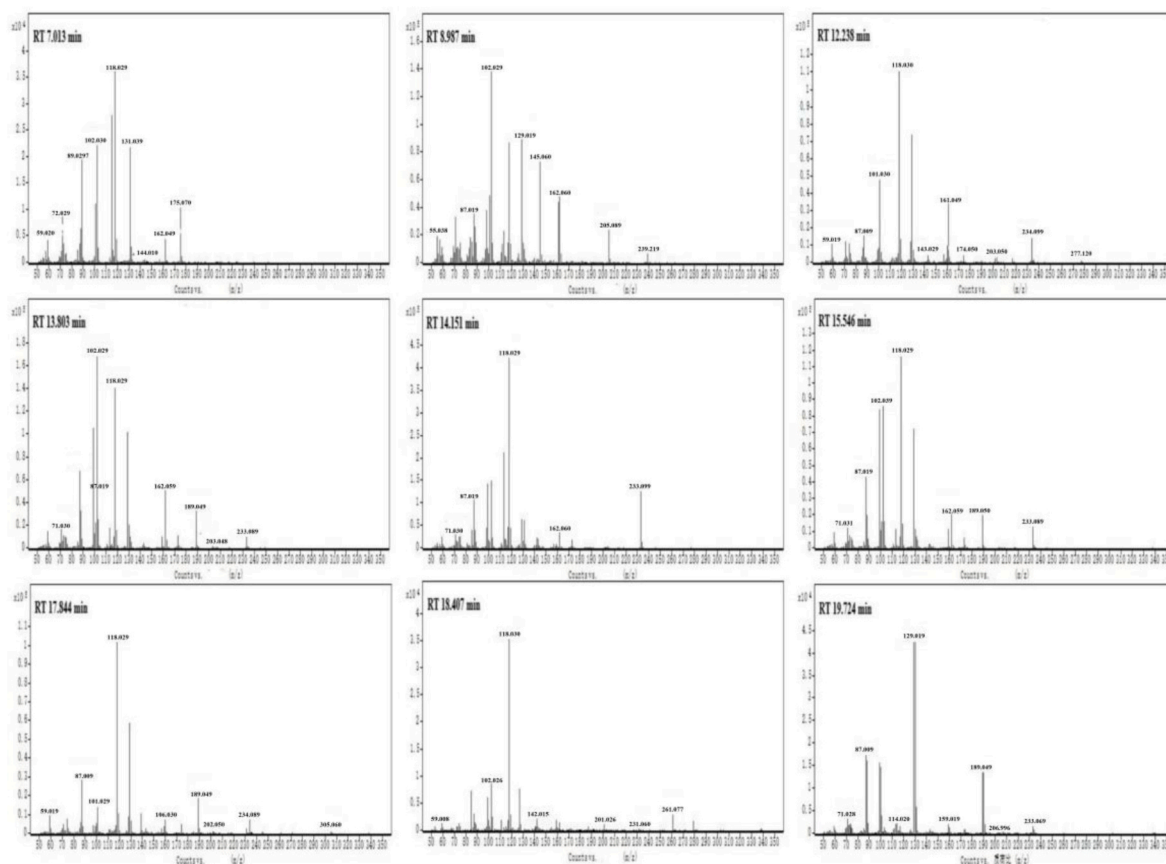


Fig. 5. Methylation results of FHEP.

3.3.2. NMR analysis

We performed an NMR analysis to determine the anomeric configuration, glycosidic bond connection mode, and connection order of polysaccharides by recording the chemical shifts of protons and carbon atoms under high-frequency magnetic fields. In the 1D NMR spectra ^1H and ^{13}C NMR were primarily present. The might be used to assign chemical shifts in carbon and hydrogen in glycosyl residues. Due to the severe signal overlap of the same atoms in 1D NMR, the molecular structure determination of polysaccharides by means of 2D NMR

techniques, such as COSY, HSQC, NOESY, and HMBC, becomes necessary.

At 3–6 ppm, the signals of polysaccharides in ^1H NMR were concentrated. The anomeric hydrogen signal of the β -glycosidic bond configuration was mainly distributed in δ 4.4–4.8 ppm, and the anomeric hydrogen signal of the α -glycosidic bond configuration was typically distributed in δ 4.8–5.8 ppm (Miao et al., 2020). As shown in Fig. 6a, the hydrogen spectrum signal of HEP was concentrated between δ 3.0–5.5 ppm, and four coupled signal peaks were identified in the

Table 2
The methylation analysis of polysaccharide.

	Type of linkage	Major mass fragments (m/z)	RT/min	Molar ratio/%
HEP	t-Glc(p)	59.03, 71.04, 87.01, 102.05, 118.04, 145.06, 162.07, 205.10	8.915	24.58
	3-Glc(p)	59.02, 87.01, 101.03, 118.04, 143.03, 161.05, 174.07, 203.07, 234.09, 277.11	12.163	20.20
	6-Glc(p)	71.03, 87.02, 102.05, 118.04, 162.06, 189.05, 203.07, 233.10	13.724	24.59
	4-Glc(p)	71.03, 87.02, 118.03, 162.06, 233.08	14.072	30.63
	FHEP	t-Fuc(p)	59.03, 72.02, 89.02, 102.03, 118.02, 131.03, 144.01, 162.04, 175.07	7.013
FHEP	t-Glc(p)	55.03, 87.00, 102.02, 129.01, 145.06, 162.06, 205.08, 239.21	8.987	19.82
	3-Glc(p)	59.01, 87.00, 101.03, 118.03, 143.02, 161.04, 174.05, 203.05, 234.09, 277.12	12.238	7.59
	6-Glc(p)	71.03, 87.01, 102.02, 118.02, 162.05, 189.04, 203.04, 233.08	13.803	15.64
	4-Glc(p)	71.03, 87.01, 118.02, 162.06, 233.09	14.151	30.03
	6-Gal(p)	71.03, 87.01, 102.03, 118.02, 162.05, 189.05, 233.08	15.546	10.25
	3,6-Glc(p)	59.01, 87.00, 101.02, 118.02, 160.03, 189.04, 202.05, 234.08, 305.06	17.844	5.56
	4,6-Glc(p)	59.00, 102.02, 118.03, 142.01, 201.02, 231.06, 261.07	18.407	3.56
	2,6-Gal(p)	71.02, 87.00, 114.02, 129.01, 159.01, 189.04, 206.99, 233.06	19.724	3.36

anomeric signal region, indicating that the sample contained at least four glycosyl residues. These residues, were marked as residues: A, B, C, and D with chemical shifts corresponding to the anomeric hydrogen δ 5.32 ppm, δ 4.55 ppm, δ 5.18 ppm, and δ 4.89 ppm, respectively. The non-anomeric hydrogen signals were concentrated in the δ 3.0–4.2 ppm region. Due to the large overlap of individual signals, combining the COSY (Fig. 6c) and HSQC (Fig. 6e) spectra became necessary to assign the H2–H6 chemical shifts of each glycosyl residue respectively. Compared to ^1H NMR, HEP identified multiple signal peaks in ^{13}C NMR (Fig. 6b), a wider shift in the chemical signal distribution was observed, and the anomeric carbon signal was concentrated between δ 90–110 ppm. The anomeric carbon signals of residues A, B, C, and D were determined to be δ 99.51 ppm, δ 96.10 ppm, δ 92.50 ppm, and δ 98.58 ppm, respectively, by ^{13}C NMR examinations and cross-peaks in the anomeric region of HSQC. The results of the monosaccharide composition, methylation analysis, anomeric signals and comprehensive reports from previous studies (Huo et al., 2020; Miao et al., 2020; H. Zhang, Wang, et al., 2020; Zhou, Huang, & Chen, 2021), it was determined that residue A was $\rightarrow 4$ - α -D-Glcp(1 \rightarrow), residue B was $\rightarrow 3$ - β -D-Glcp(1 \rightarrow), residue C was $\rightarrow 6$ - α -D-Glcp(1 \rightarrow), residue D was α -D-Glcp(1 \rightarrow). The chemical shifts of each residue were assigned using a combination of ^1H NMR, ^{13}C NMR, COSY, NOESY, HSQC and HMBC (Fig. 6), the chemical shifts of each residue were assigned respectively, and the results were shown in Table 3.

The existing structure and the connection mode of the polysaccharide were analyzed using the chemical shifts of ^{13}C and ^1H of each saccharide residue in the sample, combined with HMBC (Fig. 6f). The structure and connection mode of the polysaccharide were analyzed.

The HMBC spectrum revealed that H1 (5.32 ppm) of glycosyl residue A and C4 (76.95 ppm) of residue A had coupling signals; as did C1 (99.51 ppm) of glycosyl residue B and H4 (3.58 ppm) of residue A there was a coupled signal. There was a coupling signal for H1 (5.18 ppm) of

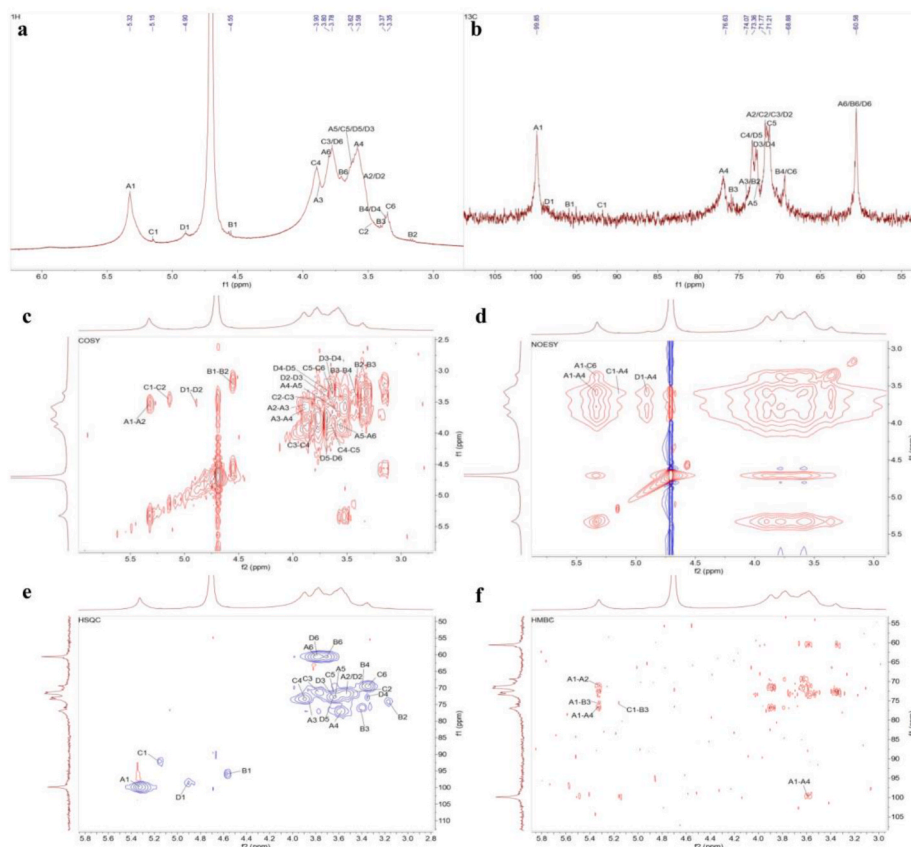


Fig. 6. NMR spectra of HEP: (A) ^1H (B) ^{13}C (C) COSY (D) NOESY (E) HSQC (F) HMBC.

Table 3
NMR signal attribution of HEP and FHEP glycosidic bond.

Code	Glycosyl residues	Chemical shifts(ppm)					
		H1/C1	H2/C2	H3/C3	H4/C4	H5/C5	H6a, b/C6
HEP	A →4)-α-D-Glcp(1→	5.32	3.52	3.86	3.58	3.62	3.8
		99.51	71.92	74.71	76.96	72.64	60.37
	B →3)-β-D-Glcp(1→	4.55	3.17	3.41	3.37	N.D.	3.7
		96.1	74.5	75.98	69.4	N.D.	60.67
FHEP	C →6)-α-D-Glcp(1→	5.18	3.46	3.78	3.9	3.64	3.35
		92.5	72	72	73.4	71	69.59
	D α-D-Glcp(1→	4.89	3.5	3.63	3.36	3.66	3.76
		98.58	71.7	73.29	72.78	73.39	60.82
	A α-D-Glcp(1→	5.23	3.87	4.03	4.12	4.45	4.34/4.45
		97.17	75.06	70.62	72.46	72.61	62.03
	B →3)-α-D-Glcp(1→	5.95	4.26	4.23	4.15	4.45	4.33/4.47
		100.74	72.62	78.84	69.28	72.67	62.05
	C →4)-α-D-Glcp(1→	5.84	4.17	3.99	4.05	4.43	4.49
		93.13	69.62	71.13	76.92	72.78	62.12
	D →6)-α-D-Glcp(1→	5.1	3.94	4.13	4.27	4.46	4.61
	103.76	74.11	74.49	72.5	69.89	70.45	
E →6)-α-D-Galp(1→	5.58	4.23	N.D.	N.D.	N.D.	4.47	
	99.28	75.68	N.D.	N.D.	N.D.	69.91	
F →3,6)-α-D-Glcp(→	5.69	4.47	4.33	4.26	3.87	4.77	
	102.09	69.83	73.48	72.46	73.84	69.83	
G →4,6)-α-D-Glcp(→	5.39	4.17	N.D.	4.23	N.D.	4.64	
	103.42	72.36	N.D.	75.39	N.D.	70.42	
H α-D-Fucp(1→	5.83	4.32	N.D.	N.D.	4.77	1.86	
	94.86	72.36	N.D.	N.D.	N.D.	16.53	
I →2,6)-α-D-Galp(1→	5.77	4.48	4.04	4.58	N.D.	4.46	
	102.04	78.22	67.96	74.31	N.D.	69.96	

“N.D.” means undetermined or not detected.

glycosyl residue C and C3 of residue B (75.67 ppm). The connection sequence of each residue in the polysaccharide was verified using the NOESY (Fig. 6d) spectrum. There was a cross peak δ 5.32/3.58 ppm cross peak between glycosyl residues A-H1 and residues C-H6; a cross peak δ 5.18/3.58 ppm cross peak between glycosyl residue C-H1 and residue A-H4; a cross peak between glycosyl residues A-H1 and residues A-H4; a cross

peak δ5.32/3.35 ppm cross peak between glycosyl residues A-H1 and residues C-H6; a cross peak δ 5.18/3.58 ppm cross peak between glycosyl residue C-H1 and residue A-H4; the glycosyl residues D-H1 and A-H4 have cross peaks δ 4.89/3.58 ppm.

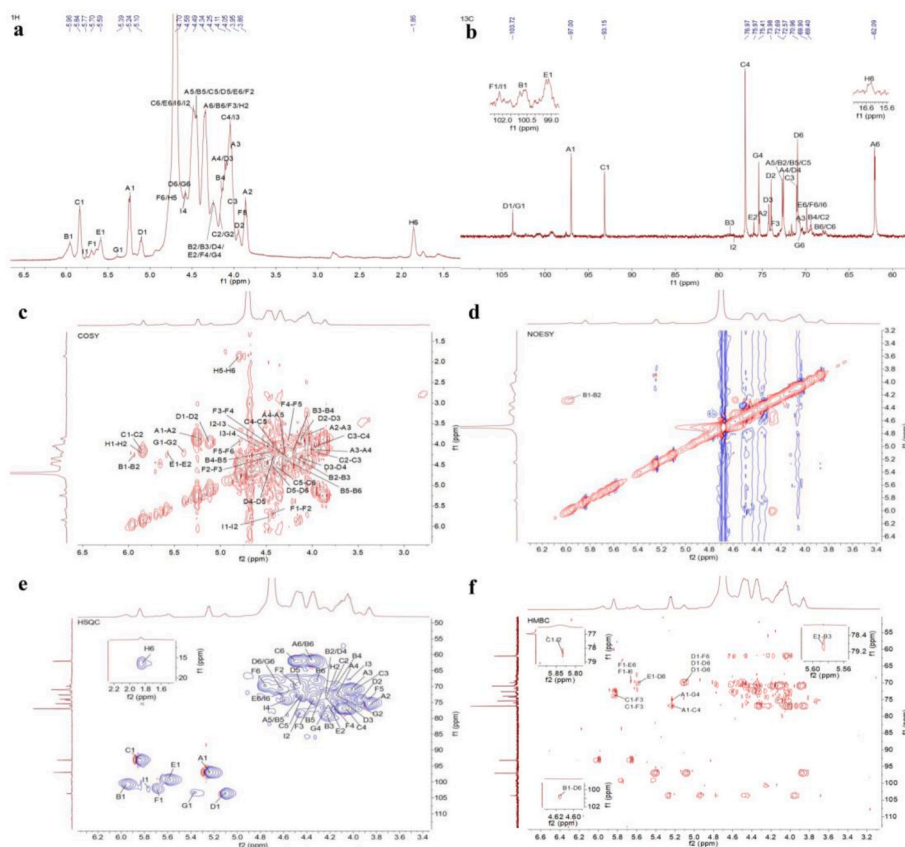


Fig. 7. NMR spectra of FHEP: (A) ¹H (B) ¹³C (C) COSY (D) NOESY (E) HSQC (F) HMBC.

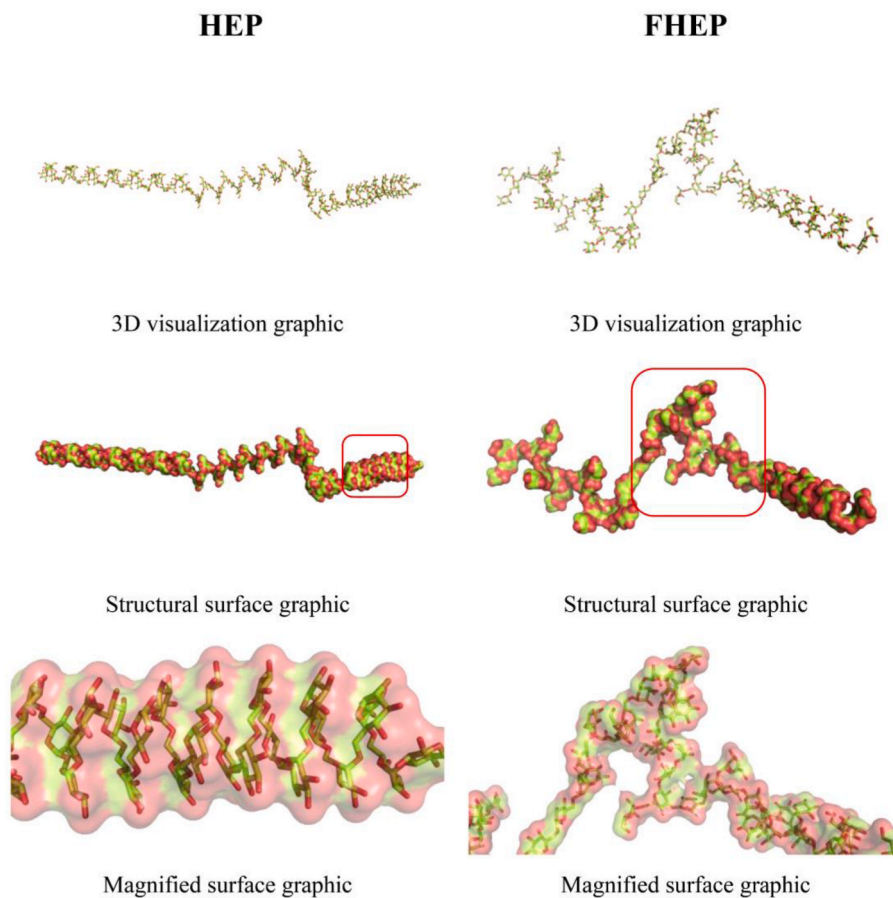


Fig. 9. Molecular simulation structure of HEP and FHEP.

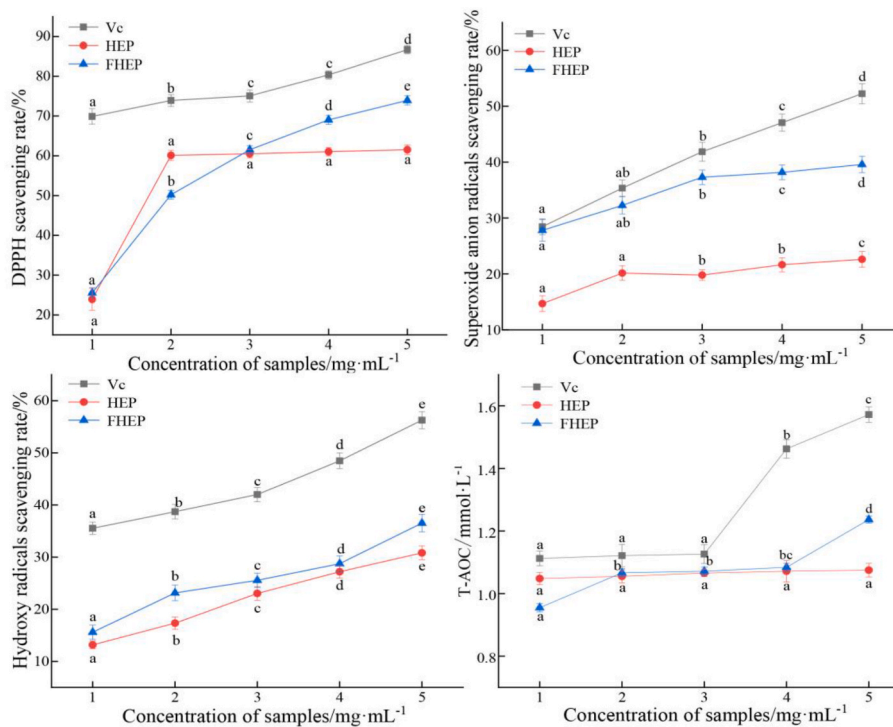


Fig. 10. In vitro antioxidant activity of HEP and FHEP.

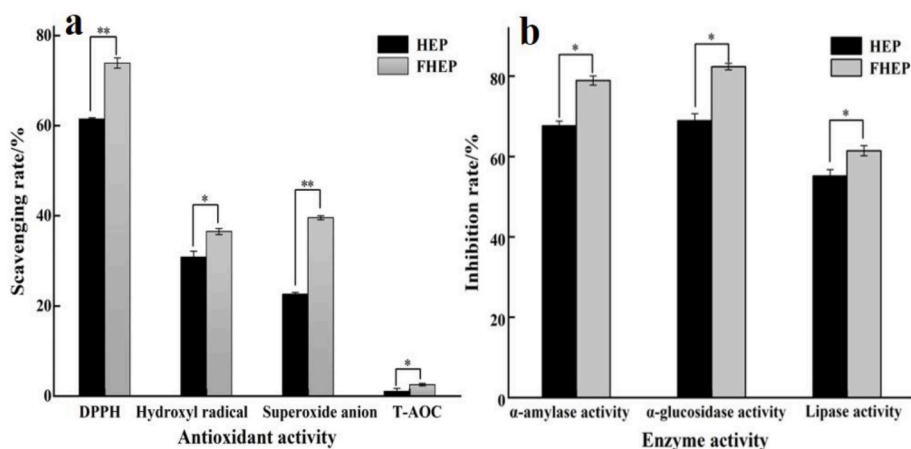


Fig. 11. In vitro biological activity of HEP and FHEP (a) antioxidant activity (b) enzyme inhibitory activity.

HEP, and FHEP for inhibiting α -glucosidase activity, were 13.83, 0.65, and 13.92, respectively. The inhibition rates of HEP on α -amylase, α -glucosidase and pancreatic lipase were 67.66%, 68.96% and 55.15%, respectively; The inhibition rates of HEP on α -amylase, α -glucosidase and pancreatic lipase were 78.93%, 82.36% and 61.43%, respectively. The results showed that, when compared to HEP, FHEP inhibited the activities of the three enzymes significantly higher ($P < 0.05$). In vitro antioxidant experiments showed that the FHEP has significantly higher antioxidant activity than HEP. According to Li et al., polysaccharides' blood lipid-lowering and blood sugar-lowering mechanisms were closely related to their antioxidant activity (Li et al., 2020). This study demonstrates that the degraded polysaccharides had better biological activity.

4. Conclusion

This was the first study showed that *Lactobacillus gasseri* JM1 degrades polysaccharides in *Hericium erinaceus*. We found that the polysaccharide degraded during the fermentation of *Hericium erinaceus* by *Lactobacillus gasseri* JM1, thereby changed its molecular weight, monosaccharide composition and structure. Compared with HEP, FHEP had a smaller molecular weight and a smaller number of monosaccharides. We performed methylation and NMR spectroscopy to analysis the structure and, found differences in the structure of the two polysaccharides. In contrast to FHEP, which had more side-chain polysaccharides with more branched chains, HEP was a polysaccharide without branched chains. The biological activity of polysaccharides with more branched chains was higher. In vitro biological activity results also showed that the three activities of FHEP were significantly higher than that of HEP. In conclusion, the polysaccharides produced greater biological activity after degradation by *Lactobacillus gasseri* JM1 compared to unfermented ones. Therefore, the future extraction and use of polysaccharides might benefit from the fermentation of *Lactobacillus gasseri* JM1.

CRedit authorship contribution statement

Yue Su: Data curation, Writing – original draft. **Hongxuan Li:** Methodology. **Ziyu Hu:** Formal analysis. **Yu Zhang:** Software. **Ling Guo:** Software. **Meili Shao:** Project administration. **Chaoxin Man:** Conceptualization. **Yujun Jiang:** All authors discussed and commented the results and gave their final approval for submission.

Declaration of competing interest

The authors have declared no conflict of interest.

Data availability

No data was used for the research described in the article.

Acknowledgement

This work was supported by the National Natural Science Foundation of China (No. 32172231).

References

- Amarita, F., Requena, T., Taborda, G., Amigo, L., & Pelaez, C. (2001). *Lactobacillus casei* and *Lactobacillus plantarum* initiate catabolism of methionine by transamination. *Journal of Applied Microbiology*, 90(6), 971–978. <https://doi.org/10.1046/j.1365-2672.2001.01331.x>
- Chen, X., Ji, H., Xu, X., & Liu, A. (2019). Optimization of polysaccharide extraction process from *grifola frondosa* and its antioxidant and anti-tumor research. *Journal of Food Measurement and Characterization*, 13(1), 144–153. <https://doi.org/10.1007/s11694-018-9927-9>
- Chen, Y., Wang, T., Zhang, X., Zhang, F., & Linhardt, R. J. (2021). Structural and immunological studies on the polysaccharide from spores of a medicinal entomogenous fungus *Paecilomyces cicadae*. *Carbohydrate Polymers*, 254, Article 117462. <https://doi.org/10.1016/j.carbpol.2020.117462>
- Chi, Y., Li, Y., Zhang, G., Gao, Y., Ye, H., Gao, J., et al. (2018). Effect of extraction techniques on properties of polysaccharides from *Enteromorpha prolifera* and their applicability in iron chelation. *Carbohydrate Polymers*, 181, 616–623. <https://doi.org/10.1016/j.carbpol.2017.11.104>
- Di Guida, R., Casillo, A., Stellavato, A., Kawai, S., Ogawa, T., Di Meo, C., et al. (2022). Capsular polysaccharide from a fish-gut bacterium induces/promotes apoptosis of colon cancer cells in vitro through Caspases' pathway activation. *Carbohydrate Polymers*, 278, Article 118908. <https://doi.org/10.1016/j.carbpol.2021.118908>
- Gao, H., Wen, J.-J., Hu, J.-L., Nie, Q.-X., Chen, H.-H., Xiong, T., et al. (2018). Polysaccharide from fermented *Momordica charantia* L. with *Lactobacillus plantarum* NCU116 ameliorates type 2 diabetes in rats. *Carbohydrate Polymers*, 201, 624–633. <https://doi.org/10.1016/j.carbpol.2018.08.075>
- Huang, F., Liu, Y., Zhang, R., Bai, Y., Dong, L., Liu, L., et al. (2019). Structural characterization and in vitro gastrointestinal digestion and fermentation of litchi polysaccharide. *International Journal of Biological Macromolecules*, 140, 965–972. <https://doi.org/10.1016/j.ijbiomac.2019.08.170>
- Huo, J., Wu, J., Sun, B., Zhao, M., Sun, W., Sun, J., et al. (2020). Isolation, purification, structure characterization of a novel glucan from Huangshui, a byproduct of Chinese Baijiu, and its immunomodulatory activity in LPS-stimulated THP-1 cells. *International Journal of Biological Macromolecules*, 161, 406–416. <https://doi.org/10.1016/j.ijbiomac.2020.06.028>
- Ji, X., Yan, Y., Hou, C., Shi, M., & Liu, Y. (2019). Structural characterization of a galacturonic acid-rich polysaccharide from *Ziziphus Jujuba cv. Muzao*. *Journal of Biological Macromolecules*, 147.
- Li, Q., Li, X., Ren, Z., Wang, R., Zhang, Y., Li, J., et al. (2021). Physicochemical properties and antioxidant activity of Maillard reaction products derived from *Dioscorea opposita* polysaccharides. *Lebensmittel-Wissenschaft und -Technologie*, 149, Article 111833. <https://doi.org/10.1016/j.lwt.2021.111833>
- Li, L., Su, Y., Feng, Y., & Hong, R. (2020). A comparison study on digestion, anti-inflammatory and functional properties of polysaccharides from four *Auricularia* species. *International Journal of Biological Macromolecules*, 154, 1074–1081. <https://doi.org/10.1016/j.ijbiomac.2020.02.324>
- Liu, Y., Zhou, Y., Liu, M., Wang, Q., & Li, Y. (2018). Extraction optimization, characterization, antioxidant and immunomodulatory activities of a novel polysaccharide from the wild mushroom *Paxillus involutus*. *International Journal of*

- Biological Macromolecules*, 112, 326–332. <https://doi.org/10.1016/j.ijbiomac.2018.01.132>
- Lopes, S. M. S., Krausová, G., Carneiro, J. W. P., Gonçalves, J. E., Gonçalves, R. A. C., & de Oliveira, A. J. B. (2017). A new natural source for obtainment of inulin and fructo-oligosaccharides from industrial waste of *Stevia rebaudiana* Bertoni. *Food Chemistry*, 225, 154–161. <https://doi.org/10.1016/j.foodchem.2016.12.100>
- Marco, M. L., Heeney, D., Binda, S., Cifelli, C. J., Cotter, P. D., Foligné, B., et al. (2017). Health benefits of fermented foods: Microbiota and beyond. *Current Opinion in Biotechnology*, 44, 94–102. <https://doi.org/10.1016/j.copbio.2016.11.010>
- Ma, J., Xu, C., Yu, H., Feng, Z., Yu, W., Gu, L., et al. (2021). Electro-encapsulation of probiotics in gum Arabic-pullulan blend nanofibres using electrospinning technology. *Food Hydrocolloids*, 111, Article 106381. <https://doi.org/10.1016/j.foodhyd.2020.106381>
- Miao, J., Regenstein, J. M., Qiu, J., Zhang, J., Zhang, X., Li, H., et al. (2020). Isolation, structural characterization and bioactivities of polysaccharides and its derivatives from *Auricularia-A* review. *International Journal of Biological Macromolecules*, 150, 102–113. <https://doi.org/10.1016/j.ijbiomac.2020.02.054>
- Mingyi, Y., Belwal, T., Devkota, H. P., Li, L., & Luo, Z. (2019). Trends of utilizing mushroom polysaccharides (MPs) as potent nutraceutical components in food and medicine: A comprehensive review. *Trends in Food Science & Technology*, 92, 94–110. <https://doi.org/10.1016/j.tifs.2019.08.009>
- Niu, J., Wang, S., Wang, B., Chen, L., Zhao, G., Liu, S., et al. (2020). Structure and anti-tumor activity of a polysaccharide from *Bletilla ochracea* Schltr. *International Journal of Biological Macromolecules*, 154, 1548–1555. <https://doi.org/10.1016/j.ijbiomac.2019.11.039>
- Pei, F., Cao, X., Wang, X., Ren, Y., & Ge, J. (2022). Structural characteristics and bioactivities of polysaccharides from blue honeysuckle after probiotic fermentation. *Lebensmittel-Wissenschaft und -Technologie*, 165, Article 113764. <https://doi.org/10.1016/j.lwt.2022.113764>
- Qi, H., Zhao, T., Zhang, Q., Li, Z., Zhao, Z., & Xing, R. (2005). Antioxidant activity of different molecular weight sulfated polysaccharides from *Ulva pertusa* Kjellm (Chlorophyta). *Journal of Applied Phycology*, 17(6), 527–534.
- Qu, H., Gao, X., Zhao, H.-T., Wang, Z.-Y., & Yi, J.-J. (2019). Structural characterization and in vitro hepatoprotective activity of polysaccharide from pine nut (*Pinus koraiensis* Sieb. et Zucc.). *Carbohydrate Polymers*, 223, Article 115056. <https://doi.org/10.1016/j.carbpol.2019.115056>
- Ryu, S. H., Hong, S. M., Khan, Z., Lee, S. K., Vishwanath, M., Turk, A., et al. (2021). Neurotrophic isoindolinones from the fruiting bodies of *Hericium erinaceus*. *Bioorganic & Medicinal Chemistry Letters*, 31, Article 127714. <https://doi.org/10.1016/j.bmcl.2020.127714>
- Sheng, Z., Wen, L., & Yang, B. (2022). Structure identification of a polysaccharide in mushroom *Lingzhi* spore and its immunomodulatory activity. *Carbohydrate Polymers*, 278, Article 118939. <https://doi.org/10.1016/j.carbpol.2021.118939>
- Sims, I. M., Carnachan, S. M., Bell, T. J., & Hinkley, S. F. R. (2018). Methylation analysis of polysaccharides: Technical advice. *Carbohydrate Polymers*, 188, 1–7. <https://doi.org/10.1016/j.carbpol.2017.12.075>
- Su, Y., & Li, L. (2020). Structural characterization and antioxidant activity of polysaccharide from four *auriculariales*. *Carbohydrate Polymers*, 229, Article 115407. <https://doi.org/10.1016/j.carbpol.2019.115407>
- Sun, L., Tian, W., Guo, X., Zhang, Y., Liu, X., Li, X., et al. (2020). *Lactobacillus gasseri* JM1 with potential probiotic characteristics alleviates inflammatory response by activating the PI3K/Akt signaling pathway in vitro. *Journal of Dairy Science*, 103(9), 7851–7864. <https://doi.org/10.3168/jds.2020-18187>
- Wang, B.-H., Cao, J.-J., Zhang, B., & Chen, H.-Q. (2019). Structural characterization, physicochemical properties and α -glucosidase inhibitory activity of polysaccharide from the fruits of wax apple. *Carbohydrate Polymers*, 211, 227–236. <https://doi.org/10.1016/j.carbpol.2019.02.006>
- Wang, L., Liu, H.-M., Xie, A.-J., Wang, X.-D., Zhu, C.-Y., & Qin, G.-Y. (2018). Chinese quince (*Chaenomeles sinensis*) seed gum: Structural characterization. *Food Hydrocolloids*, 75, 237–245. <https://doi.org/10.1016/j.foodhyd.2017.08.001>
- Wang, Y. F., Zhang, J. C., Xiao, J. B., ... Macromol, X. J. I. J. B. (2010). *Study on the purification and characterization of a polysaccharide conjugate from tea flowers*.
- Wang, L., Zhao, Z., Zhao, H., Liu, M., Lin, C., Li, L., et al. (2022). Pectin polysaccharide from *Flos Magnoliae* (Xin Yi, *Magnolia biondii* Pamp. flower buds): Hot-compressed water extraction, purification and partial structural characterization. *Food Hydrocolloids*, 122, Article 107061. <https://doi.org/10.1016/j.foodhyd.2021.107061>
- Wu, F., & Huang, H. (2021). Surface morphology and protective effect of *Hericium erinaceus* polysaccharide on cyclophosphamide-induced immunosuppression in mice. *Carbohydrate Polymers*, 251, Article 116930. <https://doi.org/10.1016/j.carbpol.2020.116930>
- Yang, M. H. D., Cui, Z., Li, H., Man, C., & Jiang, Y. (2021). Lipid-lowering effects of *Inonotus obliquus* polysaccharide in vivo and in vitro. *Foods*, 10(12), 3085.
- Yang, X., Ren, Y., & Li, L. (2022). The relationship between charge intensity and bioactivities/processing characteristics of exopolysaccharides from lactic acid bacteria. *Lebensmittel-Wissenschaft und -Technologie*, 153, Article 112345. <https://doi.org/10.1016/j.lwt.2021.112345>
- Yuan, Y., Xu, X., Jing, C., Zou, P., Zhang, C., & Li, Y. (2018). Microwave assisted hydrothermal extraction of polysaccharides from *Ulva prolifera*: Functional properties and bioactivities. *Carbohydrate Polymers*, 181, 902–910. <https://doi.org/10.1016/j.carbpol.2017.11.061>
- Yu, Y., Hu, Q., Liu, J., Su, A., Xu, H., Li, X., et al. (2021). Isolation, purification and identification of immunologically active peptides from *Hericium erinaceus*. *Food and Chemical Toxicology*, 151, Article 112111. <https://doi.org/10.1016/j.fct.2021.112111>
- Zhang, Z. H., Fan, S., Huang, D. F., Yu, Q., Liu, X. Z., Li, C., et al. (2018). *The effect of Lactobacillus plantarum NCU116 fermentation on Asparagus officinalis polysaccharide: Characterization, antioxidative, and immunoregulatory activities* (Vol. 66).
- Zhang, H., Li, C., Ding, J., Lai, P. F. H., Xia, Y., & Ai, L. (2020). Structural features and emulsifying stability of a highly branched arabinogalactan from immature peach (*Prunus persica*) exudates. *Food Hydrocolloids*, 104, Article 105721. <https://doi.org/10.1016/j.foodhyd.2020.105721>
- Zhang, Y., Liu, W., Wei, Z., Yin, B., Man, C., & Jiang, Y. (2021). Enhancement of functional characteristics of blueberry juice fermented by *Lactobacillus plantarum*. *Lebensmittel-Wissenschaft und -Technologie*, 139, Article 110590. <https://doi.org/10.1016/j.lwt.2020.110590>
- Zhang, Y., Wang, H., Guo, Q., Wang, J., & Cui, S. W. (2020). Structural characterization and conformational properties of a polysaccharide isolated from *Dendrobium nobile* Lindl. *Food Hydrocolloids*, 98, Article 104904. <https://doi.org/10.1016/j.foodhyd.2019.01.044>
- Zhou, S., Huang, G., & Chen, G. (2021). Extraction, structural analysis, derivatization and antioxidant activity of polysaccharide from Chinese yam. *Food Chemistry*, 361, Article 130089. <https://doi.org/10.1016/j.foodchem.2021.130089>
- Zhu, Z., Chen, J., Chen, Y., Ma, Y., Yang, Q., Fan, Y., et al. (2022). Extraction, structural characterization and antioxidant activity of turmeric polysaccharides. *Lebensmittel-Wissenschaft und -Technologie*, 154, Article 112805. <https://doi.org/10.1016/j.lwt.2021.112805>
- Zhu, M., Huang, R., Wen, P., Song, Y., He, B., Tan, J., et al. (2021). Structural characterization and immunological activity of pectin polysaccharide from kiwano (*Cucumis metuliferus*) peels. *Carbohydrate Polymers*, 254, Article 117371. <https://doi.org/10.1016/j.carbpol.2020.117371>